

This copy is for your personal, non-commercial use only.

If you wish to distribute this article to others, you can order high-quality copies for your colleagues, clients, or customers by [clicking here](#).

Permission to republish or repurpose articles or portions of articles can be obtained by following the guidelines [here](#).

The following resources related to this article are available online at www.sciencemag.org (this information is current as of August 3, 2010):

Updated information and services, including high-resolution figures, can be found in the online version of this article at:

<http://www.sciencemag.org/cgi/content/full/329/5990/413>

Supporting Online Material can be found at:

<http://www.sciencemag.org/cgi/content/full/science.1190897/DC1>

A list of selected additional articles on the Science Web sites **related to this article** can be found at:

<http://www.sciencemag.org/cgi/content/full/329/5990/413#related-content>

This article **cites 36 articles**, 14 of which can be accessed for free:

<http://www.sciencemag.org/cgi/content/full/329/5990/413#otherarticles>

This article has been **cited by 1** articles hosted by HighWire Press; see:

<http://www.sciencemag.org/cgi/content/full/329/5990/413#otherarticles>

This article appears in the following **subject collections**:

Neuroscience

<http://www.sciencemag.org/cgi/collection/neuroscience>

Genetic Reactivation of Cone Photoreceptors Restores Visual Responses in Retinitis Pigmentosa

Volker Busskamp,^{1,2*} Jens Duebel,^{1*} David Balya,^{1*} Mathias Fradot,^{3,4,5} Tim James Viney,¹ Sandra Siegert,¹ Anna C. Groner,^{2,6} Erik Cabuy,¹ Valérie Forster,^{3,4,5} Mathias Seeliger,⁷ Martin Biel,⁸ Peter Humphries,⁹ Michel Paques,^{3,4,5,10,11} Saddek Mohand-Said,^{3,4,5,10} Didier Trono,^{2,6} Karl Deisseroth,¹² José A. Sahel,^{3,4,5,10,11} Serge Picaud,^{3,4,5,11} Botond Roska^{1†}

Retinitis pigmentosa refers to a diverse group of hereditary diseases that lead to incurable blindness, affecting two million people worldwide. As a common pathology, rod photoreceptors die early, whereas light-insensitive, morphologically altered cone photoreceptors persist longer. It is unknown if these cones are accessible for therapeutic intervention. Here, we show that expression of archaeobacterial halorhodopsin in light-insensitive cones can substitute for the native phototransduction cascade and restore light sensitivity in mouse models of retinitis pigmentosa. Resensitized photoreceptors activate all retinal cone pathways, drive sophisticated retinal circuit functions (including directional selectivity), activate cortical circuits, and mediate visually guided behaviors. Using human *ex vivo* retinas, we show that halorhodopsin can reactivate light-insensitive human photoreceptors. Finally, we identified blind patients with persisting, light-insensitive cones for potential halorhodopsin-based therapy.

Retinitis pigmentosa (1, 2) is the result of diverse mutations in more than 44 genes expressed in rod photoreceptors (3), which then degenerate, causing loss of night vision. Subsequently, cone photoreceptors, which are responsible for color and high-acuity daytime vision, progressively lose their photoreceptive outer segments, leading to overall blindness. Despite this loss of sensitivity, cone cell bodies remain present longer than rods in both humans and animals (4–6), but it is not known whether these light-insensitive cells can be reactivated or if information from them can still flow to downstream visual circuits (Fig. 1A) for a substantial time window after the loss of photosensitivity (7).

To restore light-evoked activity in light-insensitive cone photoreceptors, we genetically targeted a light-activated chloride pump (8–10), enhanced *Natronomonas pharaonis* halorhodopsin (eNpHR) (11, 12), to photoreceptors by means of adeno-associated viruses (AAVs) (13, 14).

Light-activated chloride pumps are rational candidates for reactivating vertebrate photoreceptors, as both eNpHR-expressing cells (12) and healthy photoreceptors hyperpolarize in response to increases in light intensity. We selected two animal models of retinitis pigmentosa for gene therapy, both of which lead to retinal degeneration (RD). *Cnga3*^{−/−}; *Rho*^{−/−} double-knockout mice served as a model of slow forms of RD (s-RD mice) (15), and *Pde6b*^{rd1} (also known as rd1) mice modeled fast forms of RD (f-RD mice) (16). Targeted expression of eNpHR was accomplished with the use of three cell-specific promoters (Fig. 1B): (i) human rhodopsin (hRHO) (17), (ii) human rod opsin (hRO) (18), and (iii) mouse cone arrestin-3 (mCAR) (19).

To assess the effectiveness and specificity of the promoters, we used eNpHR fused to enhanced yellow fluorescent protein (EYFP) (Fig. 2, A to I) (11). It is important to restrict the expression of eNpHR to photoreceptors only, because eNpHR

in downstream retinal circuit elements, such as ON-bipolar and ON-ganglion cells, may inhibit the flow of information across the retina. Enhanced green fluorescent protein (EGFP)-expressing AAVs were used as controls throughout this study (fig. S1). We selected the hRO and mCAR promoters for s-RD mice (Fig. 2, B and C) and the mCAR promoter for f-RD mice (Fig. 2F), on the basis of their ability to selectively drive expression of eNpHR-EYFP in a high percentage of cone photoreceptors (figs. S2 and S3).

The life span of cones in RD mice defines the window of opportunity for reactivation. Therefore, we tested EYFP or EGFP expression driven by the mCAR promoter at different time points during retinal degeneration. Surprisingly, EYFP and EGFP expression lasted more than eight months (Fig. 3A, fig. S4, last tested f-RD at postnatal day 264 (P264) and s-RD at P255), longer than opsin protein expression [~P95 (5) or between P21 and P110 (20)]. We isolated these long-lasting AAV-transduced cells from f-RD retinas at different time points and verified their identity by analyzing their transcriptome (P110 to P220, fig. S5). Cone-specific genes were expressed in the isolated cells, whereas markers of other retinal cell types were absent, suggesting that AAV-labeled cells are altered cones, even at later stages of degeneration. The fact that opsin mRNA remained, whereas the opsin protein did not, suggests translational down-regulation of opsins, as also shown before (20). We estimate that ~27% of cones remain between P184 and P255 in s-RD and ~25% remain between P182 and P264 in f-RD mice (Fig. 3A).

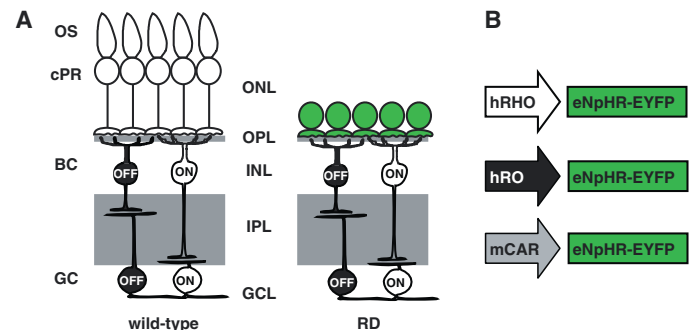
We tested whether eNpHR drives cone light responses in RD retinas at an age (P53 to P264, table S1) when many (s-RD) (15) or all (f-RD) (20) rods have already died. eNpHR-EYFP-expressing photoreceptors in s-RD and f-RD retinas displayed larger (Fig. 3B and fig. S6), more sustained (Fig. 3C), and significantly faster (Fig. 3D) photocurrents than those of wild-type (WT) cones. The photocurrents peaked at 580 nm. Photoreceptors expressing only EGFP did not

¹Neural Circuit Laboratories, Friedrich Miescher Institute for Biomedical Research, Basel, Switzerland. ²National Centre of Competence in Research Frontiers in Genetics Program, Geneva 1211, Switzerland. ³Inserm, UMR_S968, Institut de la Vision, Paris, France. ⁴Université Pierre et Marie Curie Paris 06, UMR_S968, Institut de la Vision, Paris F-75012, France. ⁵CNRS, UMR_7210, Paris F-75012, France. ⁶School of Life Sciences, Ecole Polytechnique Fédérale de Lausanne, Lausanne, Switzerland. ⁷Division of Ocular Neurodegeneration, Institute for Ophthalmic Research, Department of Ophthalmology II, Eberhard-Karls University, Tübingen, Germany. ⁸Center for Integrated Protein Science Munich and Department of Pharmacy, Ludwig-Maximilians-Universität München, Munich, Germany. ⁹Smurfit Institute of Genetics, Trinity College, Dublin, Ireland. ¹⁰Centre d'Investigation Clinique 503, Inserm-Centre Hospitalier National d'Ophthalmologie des Quinze-Vingts, Paris, France. ¹¹Fondation Ophthalmologique Adolphe de Rothschild, Paris, France. ¹²Department of Bioengineering and Department of Psychiatry and Behavioral Sciences, Stanford University, Stanford, CA 94305, USA.

*These authors contributed equally to this work.

†To whom correspondence should be addressed. E-mail: botond.roska@fmi.ch

Fig. 1. Scheme of the excitatory pathways of cone retinal circuitry in WT and RD retinas. (A) Cone photoreceptors (cPR) in WT retinas (left) detect light with photopigments in their outer segments (OS). Cone cell bodies are located in the outer nuclear layer (ONL). Cones provide input to ON and OFF bipolar cells (BC) that have cell bodies in the inner nuclear layer (INL). Bipolar cells are connected to corresponding ON and OFF ganglion cells (GC). Ganglion cell bodies are in the ganglion cell layer (GCL), and their axons relay visual information to higher visual centers. The locations of inhibitory interactions mediated by horizontal cells in the outer plexiform layer (OPL) and by amacrine cells in the IPL are indicated by gray boxes. Light-insensitive RD cones (right) lack outer segments, but their cell bodies (green) persist longer than rods. (B) AAV-expression constructs. hRHO, hRO, or mCAR promoters drive eNpHR-EYFP.



react to light. The magnitude of photocurrents in eNpHR-transduced s-RD and f-RD mice were similar (Fig. 3B). The current size was independent of the holding voltage (Fig. 3E), a finding that is consistent with the view that the photocurrents

are mediated by ion pumps (10). Photocurrents and voltages were modulated across three logarithmic units of intensities (fig. S6). In the absence of functional outer segments, which normally generate currents that depolarize photoreceptors

in the dark, RD photoreceptors were expected to stay hyperpolarized. A hyperpolarized state would limit the ability of eNpHR currents to modulate synaptic transmission. However, the recorded eNpHR-expressing RD photoreceptors were depo-

Fig. 2. Targeted expression of a light-sensitive chloride pump in persisting photoreceptors in RD retinas. (A to I) Cross sections of GFP-immunostained (35) retinas transduced by hRHO- (A, D, G), hRO- (B, E, H), and mCAR- (C, F, I) eNpHR-EYFP AAVs in s-RD (A to C), f-RD (D to F), and WT (G to I) mice. Left panel of each pair, eNpHR-EYFP; right panel of each pair, co-stained with 4',6'-diamidino-2-phenylindole (DAPI). Scale bar, 20 μ m.

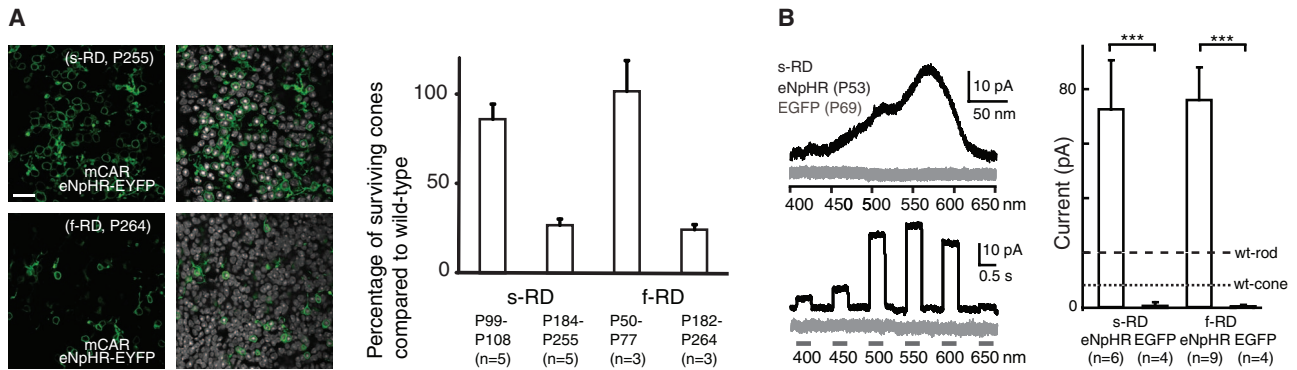
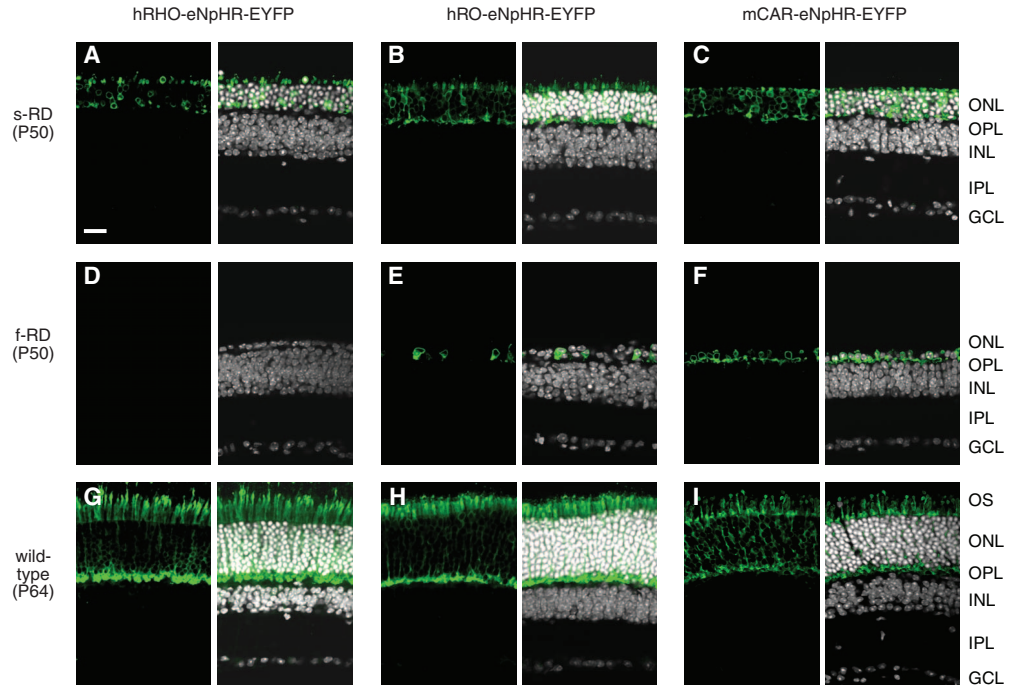


Fig. 3. Light responses in surviving eNpHR-expressing RD cones. (A) (Left) Confocal top views of GFP-immunostained RD photoreceptors transduced by mCAR-eNpHR-EYFP in P255 s-RD (top) and P264 f-RD (bottom) retinas. Left panel of each pair, eNpHR-EYFP; right panel of each pair, co-stained with DAPI. Scale bar 20 μ m. (Right) Estimated fraction of surviving cones (35) in s-RD and f-RD mice at different time points compared with WT cone numbers. n, number of retinas analyzed. (B) (Left) Photocurrent action spectrum of an eNpHR- (black) or EGFP- (gray) expressing s-RD cone. Top, color-ramp; bottom, light flashes. Gray bars indicate the timing of the full-field light stimuli. (Right) Magnitude of photocurrents in photoreceptors expressing eNpHR or EGFP. Dashed lines show the peak magnitude of photocurrents in WT cones (short dashes) and WT rods (long dashes). Stars indicate statistical significance (35). (C) Peak and steady-state photocurrents (0.5-s flash) in RD and

WT animals. (D) Rise and decay time constants of eNpHR-mediated photocurrents compared with the rise time constant in WT photoreceptors. (E) eNpHR-mediated photocurrents in RD retinas at different holding voltages. Because the response properties in s-RD and f-RD mice were similar, the data from both mouse lines were grouped in panels (C to E). All WT cone response data shown in Fig. 3 were taken from (36). Error bars indicate SEM.

larized in the dark [-26 ± 3 mV, $n = 12$ cones; see supporting online material (SOM)].

The ability of eNpHR-reactivated RD photoreceptors to convey information to downstream retinal circuits depends on the presence of functional photoreceptor-to-bipolar cell synapses. As retinal degeneration progresses, these synapses morphologically reorganize (3). However, they still possess elements of both pre- and post-synaptic machinery (5). To test for potential sig-

nal flow from photoreceptors to ganglion cells, the output neurons of the retina. Ganglion cells in eNpHR-transduced s-RD and f-RD retinas displayed robust, light-evoked excitatory currents (Fig. 4A), indicating functional outer and inner retinal synaptic connections. The magnitudes of these excitatory currents were comparable to those in WT retinas (Fig. 4A). There were no measurable light-evoked currents in the

ganglion cells of retinas transfected with EGFP (Fig. 4A).

The retina incorporates two major information channels that diverge at the level of bipolar cells and are physically separated by depth within the inner plexiform layer (IPL). ON cells are activated by light increments, whereas OFF cells are activated by light decrements (21). The activity of ganglion cells is coded by action potentials (“spikes”) that form the output signal of

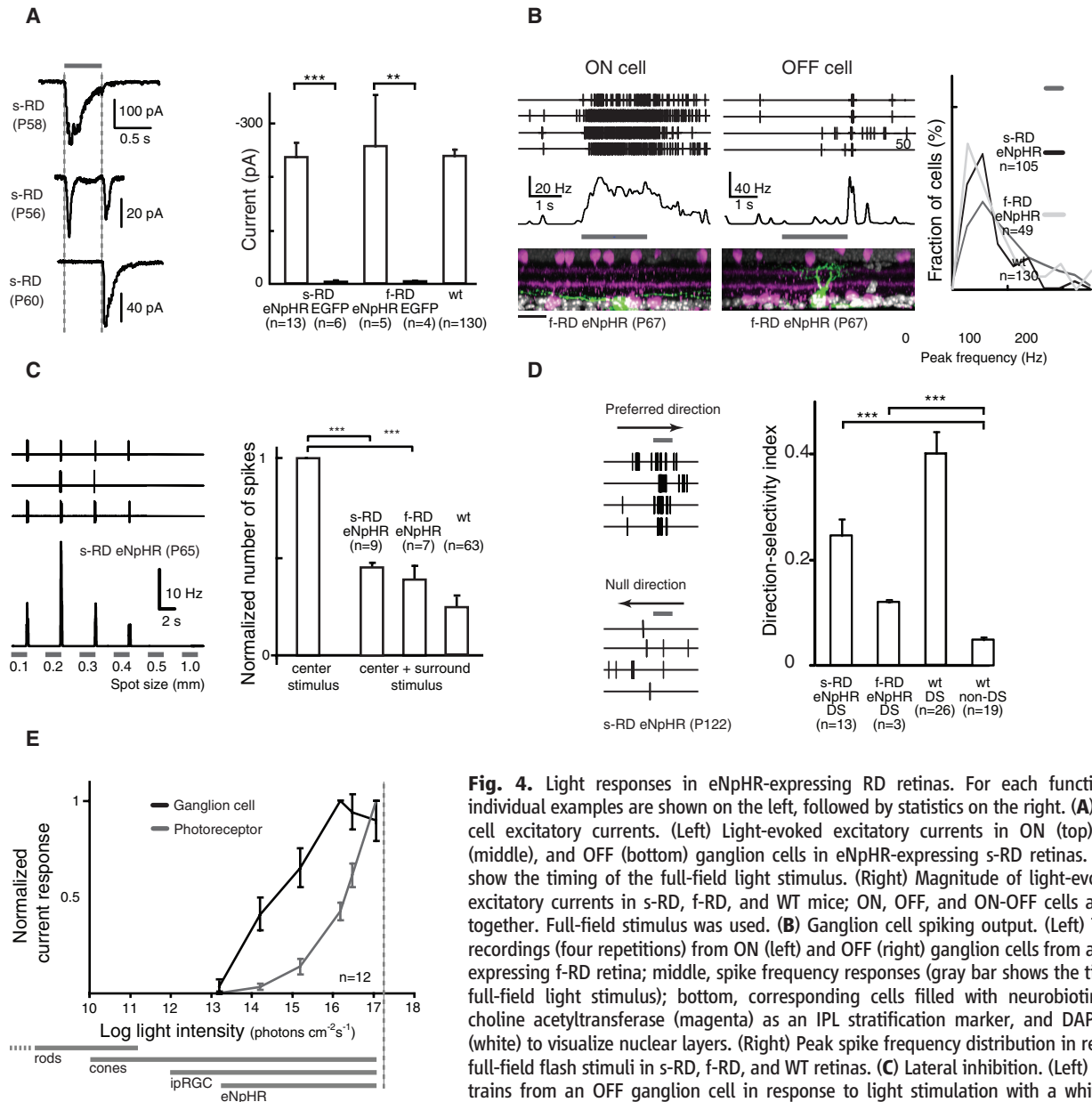


Fig. 4. Light responses in eNpHR-expressing RD retinas. For each functional test, individual examples are shown on the left, followed by statistics on the right. **(A)** Ganglion cell excitatory currents. (Left) Light-evoked excitatory currents in ON (top), ON-OFF (middle), and OFF (bottom) ganglion cells in eNpHR-expressing s-RD retinas. Gray bars show the timing of the full-field light stimulus. (Right) Magnitude of light-evoked peak excitatory currents in s-RD, f-RD, and WT mice; ON, OFF, and ON-OFF cells are pooled together. Full-field stimulus was used. **(B)** Ganglion cell spiking output. (Left) Top, spike recordings (four repetitions) from ON (left) and OFF (right) ganglion cells from an eNpHR-expressing f-RD retina; middle, spike frequency responses (gray bar shows the timing of a full-field light stimulus); bottom, corresponding cells filled with neurobiotin (green), choline acetyltransferase (magenta) as an IPL stratification marker, and DAPI staining (white) to visualize nuclear layers. (Right) Peak spike frequency distribution in response to full-field flash stimuli in s-RD, f-RD, and WT retinas. **(C)** Lateral inhibition. (Left) Top, spike trains from an OFF ganglion cell in response to light stimulation with a white spot of increasing size (three repetitions); bottom, corresponding spike frequency. (Right) Number

of spikes evoked by 1-mm-diameter spot stimuli (center + surround stimulus) relative to the number of spikes evoked by a 0.1- to 0.2-mm spot (center stimulus). **(D)** Directional selective responses. (Left) Spike recordings during stimulation with a fast-moving bar (width, 200 μm ; speed, 1.5 mm s^{-1} ; four repetitions) in the preferred direction (top) and in the opposite direction (“null” direction, bottom). Stimulus timing is shown by gray bars. (Right) Direction-selectivity index (35, 37). **(E)** Light sensitivity. eNpHR-induced excitatory current responses in ganglion cells and photocurrents in photoreceptors as a function of light intensity. The gray lines at the bottom display the ranges of sensitivities for rods (only partially shown), cones, and intrinsically photosensitive ganglion cells (ipRGCs). The maximum light intensity at 580 nm allowed in the human eye, according to the 2006 European directives on artificial optical radiation (28), is shown by the vertical dashed line. In all panels, n , number of different cells from which we took our measurements; error bars, SEM; stars, statistical significance (35). Light intensity was 10^{16} photons $\text{cm}^{-2} \text{s}^{-1}$ for each experiment.

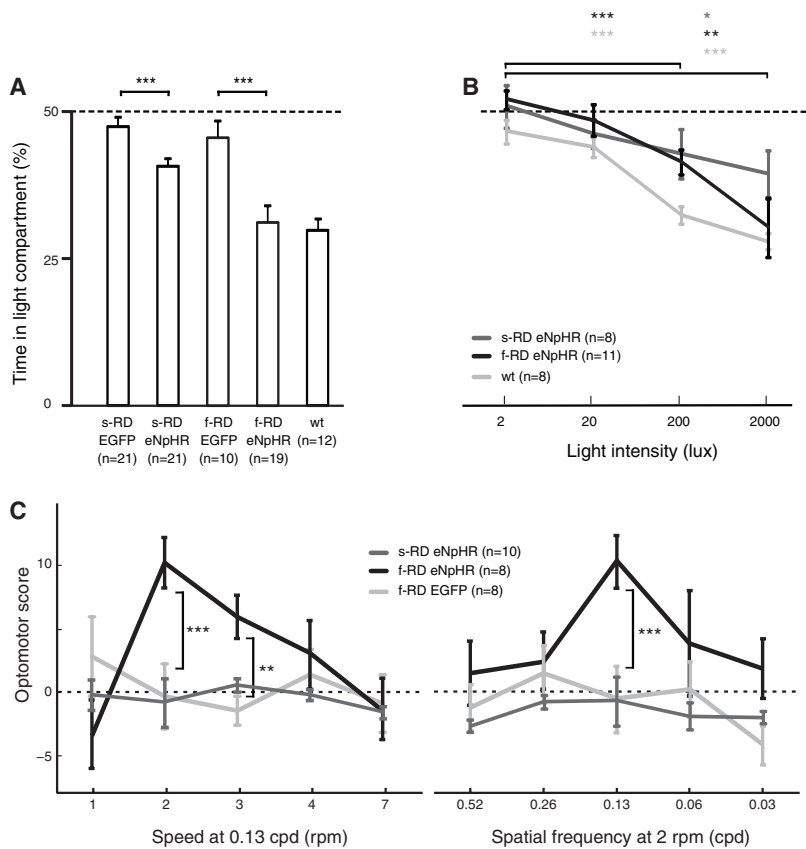


Fig. 5. Visually guided behavior in eNpHR-expressing RD mice. **(A)** Dark-light box experiment. Percentage of time the AAV-injected RD animals and WT mice spent in the light compartment. **(B)** Dark-light box test. Percentage of time mice spent in the light compartment as a function of light intensity. **(C)** Optomotor response score of eNpHR- or EGFP-expressing RD animals at different rotational speeds and spatial frequencies. rpm, revolutions per minute. In all panels, n, number of different animals; error bars, SEM; stars, statistical significance (35).

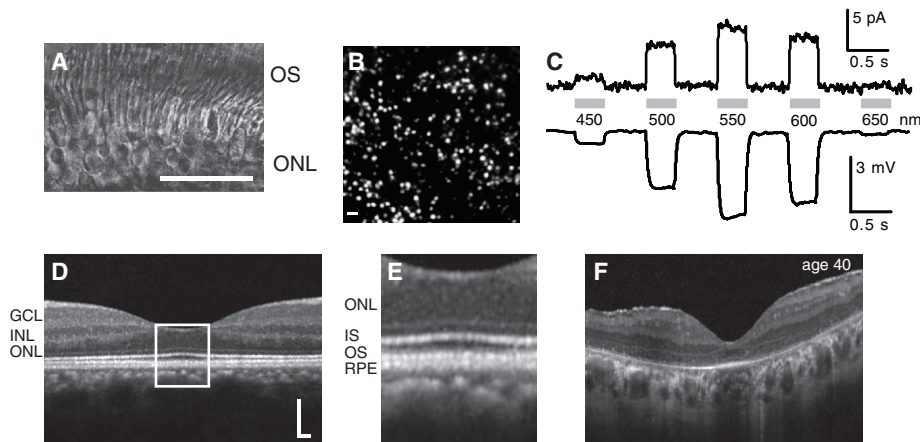


Fig. 6. Translational aspects of eNpHR-EYFP-mediated reactivation of photoreceptors. **(A)** Retinal slice from a human retinal explant (24 hours postmortem). Scale bar, 30 μ m. **(B)** Fluorescent live image of a lentivirus-transfected area from a human retina after 7 days in culture and 2 days after lentiviral administration. Scale bar, 20 μ m. **(C)** Action spectrum of an eNpHR-expressing human photoreceptor stimulated with full-field light flashes ranging from 450 to 650 nm (top, current response; bottom, voltage response). Gray bars indicate the timing of the stimulus. **(D)** Representative OCT scan covering the foveal region of a healthy individual. **(E)** Magnified image. IS, inner segments; RPE, retinal pigment epithelium. Scale bar, 200 μ m. **(F)** OCT from the left eye of a 40-year-old male patient with sporadic retinitis pigmentosa (loss of vision since the age of 15). Outer segments are undetectable.

the retina (22) and the input signal to higher brain centers. Notably, light stimulation evoked excitatory currents and spiking activity in ganglion cells of eNpHR-transduced RD retinas, either at light increments, light decrements, or both (P53 to P264; Fig. 4, A and B). The dendritic processes of morphologically reconstructed ganglion cells were properly aligned in the corresponding ON or OFF strata (23) of the IPL (Fig. 4B). Ganglion cell spike frequencies spanned similar ranges in s-RD, f-RD, and WT retinas (Fig. 4B). Some ganglion cell types respond preferentially to changes in illumination and therefore spike transiently after a light step, whereas others represent the level of illumination and thus spike in a more sustained manner. The dynamics of spiking activity in eNpHR-transduced retinas varied from transient to sustained, as in WT retinas (fig. S7). Light-stimulation of eNpHR-reactivated photoreceptors in RD retinas even evoked ganglion cell spiking activity at later stages of degeneration (s-RD: <P255, f-RD: <P264; fig. S7).

We next asked if basic forms of spatial processing were functional in the eNpHR-transduced RD retinas. Lateral inhibition is a conserved feature of vertebrate retinas that is important for spatial contrast (“edge”) enhancement. When spots of increasing sizes were presented to eNpHR-expressing RD retinas, the response magnitude of ganglion cells reached a maximum and then gradually decreased, a sign of lateral inhibition (Fig. 4C and fig. S7) (21, 24). Lateral inhibition also results in ON-center, OFF-surround responses (21) that we were able to observe in eNpHR-expressing RD retinas (fig. S7). Another example of spatial processing is the directional-selective responses of types of ganglion cells to motion stimuli (25). The activity of directional selective ganglion cells is important for the optokinetic reflex (26). When eNpHR-transduced RD retinas were stimulated with bars moving in different directions, some ganglion cells responded preferentially to motion in a particular direction but produced little activity when the bar moved in the opposite direction (Fig. 4D) (27). This response asymmetry suggests that the retinal circuit for directional selectivity is, at least partially, maintained in RD retinas.

The sensitivity of eNpHR to light is less than that of normal cones (Fig. 4E), and although normal cones can adapt to different light intensities, eNpHR-driven cones have a fixed sensitivity range (see SOM). However, the sensitivity of ganglion cells to light was 1.7 log units higher than that of the eNpHR-expressing photoreceptors (Fig. 4E), and the light levels required for eNpHR stimulation at 580 nm are below the limit allowed for safe radiation of the human eye, according to the 2006 European directives on artificial optical radiation (Fig. 4E) (28).

The slow and fast RD mouse models differ not only in the time course of photoreceptor degeneration, but also in the amount of light-driven activity present during development. s-RD mice

have no light-sensitive rod-cone system during development (15), whereas f-RD mice lose the rod-cone function gradually and are blind by 4 weeks of age (16). In the retina, the responses in eNpHR-activated s-RD and f-RD mice were similar, suggesting that the development of the tested retinal functions, like direction selectivity, may not require light-driven input from rods and cones. Light stimulation of the eyes resulted in visually evoked potentials in eNpHR-expressing f-RD mice but not in EGFP-transduced controls (P42 to P118, fig. S8). In contrast to the retina, we could not measure light-driven cortical activity in eNpHR-transduced s-RD mice.

We next evaluated whether light could induce behavioral changes in eNpHR-transduced mice. In dark-light box tests (29), eNpHR-expressing f-RD and s-RD mice performed significantly better than the corresponding EGFP-expressing control groups (P44 to P143, Fig. 5A), and the increased performance depended on the illumination level (Fig. 5B). In the optomotor reflex test (30), only eNpHR-expressing f-RD mice performed better than EGFP-expressing control mice at a variety of drum speeds (P69 to P153, Fig. 5C). WT (fig. S8) and f-RD responses both peaked at the same speed. The optimum spatial frequency was higher for WT animals [0.26 cycles per degree (cpd)] compared to f-RD (0.13 cpd). These experiments demonstrated that resensitized photoreceptors are able to drive visually guided behavior in f-RD mice and, to some extent, in s-RD mice.

To test for potential toxicity of eNpHR or the unmodified NpHR, we first compared the retinas of eNpHR-transduced WT mice (6 weeks after AAV administration) with those of normal WT mice. The number of photoreceptors was similar in both conditions (fig. S9), and, in addition to the light-induced spiking activity, ganglion cells in eNpHR-transduced WT retinas had a wider action spectrum (a gain of function at longer wavelengths) than ganglion cells in uninjected WT retinas (fig. S9). This suggests that both intrinsic opsins and eNpHR are at work. Next, we compared the retinas of transgenic mice expressing NpHR in photoreceptors under the control of a bovine rhodopsin promoter with WT retinas and found similar numbers of photoreceptors (at P140, fig. S9). These results suggest that, in the studied time window, neither the unmodified NpHR nor eNpHR induced additional photoreceptor degeneration.

The translation of gene therapy achieved in mice to human participants requires the use of promoters and AAV serotypes that drive photoreceptor-specific eNpHR expression in human retinas. Therefore, we tested our AAVs on human ex vivo retinal explants (Fig. 6A), which we could keep in culture for 2 to 3 weeks. Because of this short time window and the relatively long period of time required to efficiently express eNpHR from AAVs, we had to use immunohistochemistry to visualize eNpHR-EYFP protein expression in the cultured human retinas. Of the three promoters, mCAR directed expression of eNpHR specifi-

cally in human photoreceptors (fig. S10). To reduce the time required to obtain robust eNpHR-EYFP expression, which is necessary for two-photon laser-targeted electrophysiology, we inserted the mCAR-eNpHR construct into a lentiviral vector (fig. S10) (31). Using this new vector, we found high levels of eNpHR expression, specifically in human photoreceptors after only 1 to 2 days of incubation (Fig. 6B and fig. S10). Brightly labeled photoreceptors in the parafoveal region displayed photocurrents and photovoltages with spectral tuning reflecting eNpHR activation (Fig. 6C and fig. S10). We could not measure any photocurrents from control human retinas, even at the time when the retina was isolated.

To find potential patients with retinitis pigmentosa eligible for eNpHR-mediated restoration of visual functions, we screened a database (see SOM) that contained records of retinal images acquired by optical coherence tomography (OCT), Goldman visual field tests, multifocal electroretinograms (ERGs), full-field ERGs, and visual-acuity tests. We identified legally blind patients (data from one of whom are shown in Fig. 6 and fig. S11) with no visible outer segments on OCT pictures, but cone cell bodies in the central region. These criteria may be used in the future for selecting patients who could benefit from this therapy.

We have shown that a microbial gene introduced to surviving cone cell bodies reactivated retinal ON and OFF pathways and the retinal circuitry for lateral inhibition and directional selective responses. Moreover, the reactivated cones enabled RD mice to perform visually guided behaviors. The tested time window of intervention was up to ~260 days in f-RD and s-RD mice, suggesting that persisting cone cell bodies (~25%) are enough to induce ganglion cell activity, even during later stages of degeneration. Our finding that AAVs with the mCAR promoter specifically transduced human photoreceptors and the identification of patients with little measurable visual function and no outer segments but surviving cone cell bodies suggest a potential for translating eNpHR-based rescue of visual function to humans (see SOM). In the future, eNpHR-based restoration may be combined with other approaches that increase the survival of altered photoreceptors (20, 32–34).

References and Notes

1. K. Shintani, D. L. Shechtman, A. S. Gurwood, *Optometry* **80**, 384 (2009).
2. T. Cronin, T. Léveillard, J. A. Sahel, *Curr. Gene Ther.* **7**, 121 (2007).
3. R. E. Marc, B. W. Jones, C. B. Watt, E. Strettoi, *Prog. Retin. Eye Res.* **22**, 607 (2003).
4. Z. Y. Li, I. J. Kljavin, A. H. Milam, *J. Neurosci.* **15**, 5429 (1995).
5. B. Lin, R. H. Masland, E. Strettoi, *Exp. Eye Res.* **88**, 589 (2009).
6. A. H. Milam, Z. Y. Li, R. N. Fariss, *Prog. Retin. Eye Res.* **17**, 175 (1998).
7. E. Banin et al., *Neuron* **23**, 549 (1999).
8. E. Bamberg, J. Tittor, D. Oesterhelt, *Proc. Natl. Acad. Sci. U.S.A.* **90**, 639 (1993).
9. B. Schobert, J. K. Lanyi, *J. Biol. Chem.* **257**, 10306 (1982).

10. A. Seki et al., *Biophys. J.* **92**, 2559 (2007).
11. V. Gradinaru, K. R. Thompson, K. Deisseroth, *Brain Cell Biol.* **36**, 129 (2008).
12. F. Zhang et al., *Nature* **446**, 633 (2007).
13. G. P. Gao et al., *Proc. Natl. Acad. Sci. U.S.A.* **99**, 11854 (2002).
14. C. Leberherz, A. Maguire, W. Tang, J. Bennett, J. M. Wilson, *J. Gene Med.* **10**, 375 (2008).
15. E. Claes et al., *Invest. Ophthalmol. Vis. Sci.* **45**, 2039 (2004).
16. D. B. Farber, J. G. Flannery, C. Bowes-Rickman, *Prog. Retin. Eye Res.* **13**, 31 (1994).
17. M. Allocca et al., *J. Virol.* **81**, 11372 (2007).
18. Y. Wang et al., *Neuron* **9**, 429 (1992).
19. X. Zhu et al., *FEBS Lett.* **524**, 116 (2002).
20. C. Punzo, K. Kornacker, C. L. Cepko, *Nat. Neurosci.* **12**, 44 (2009).
21. S. W. Kuffler, *J. Neurophysiol.* **16**, 37 (1953).
22. T. Gollisch, M. Meister, *Neuron* **65**, 150 (2010).
23. E. V. Famiglietti Jr., H. Kolb, *Science* **194**, 193 (1976).
24. H. B. Barlow, *J. Physiol.* **119**, 69 (1953).
25. J. B. Demb, *Neuron* **55**, 179 (2007).
26. K. Yoshida et al., *Neuron* **30**, 771 (2001).
27. H. B. Barlow, R. M. Hill, *Science* **139**, 412 (1963).
28. P. Degenaar et al., *J. Neural Eng.* **6**, 035007 (2009).
29. M. Bourin, M. Hascoët, *Eur. J. Pharmacol.* **463**, 55 (2003).
30. J. Abdeljalil et al., *Vision Res.* **45**, 1439 (2005).
31. R. Zufferey, D. Nagy, R. J. Mandel, L. Naldini, D. Trono, *Nat. Biotechnol.* **15**, 871 (1997).
32. B. Chen, C. L. Cepko, *Science* **323**, 256 (2009).
33. T. Léveillard, J. A. Sahel, *Sci. Transl. Med.* **2**, 26ps16 (2010).
34. Y. Yang et al., *Mol. Ther.* **17**, 787 (2009).
35. Materials and methods are available as supporting material on Science Online.
36. S. S. Nikonov, R. Kholodenko, J. Lem, E. N. Pugh Jr., *J. Gen. Physiol.* **127**, 359 (2006).
37. W. R. Taylor, D. I. Vaney, *J. Neurosci.* **22**, 7712 (2002).
38. We thank B. G. Scherf, S. Djaffer, and H. Kohler for technical assistance and P. Lagali, K. Farrow, A. Matus, and S. Oakeley for their comments on the manuscript. pAAV2.1-Rho-EGFP was provided by A. Auricchio, and J. Nathans provided the pRed2.1lacZ. Post-mortem human retinas were provided by T. Wesseling and E. Pels at the Cornea Bank in Amsterdam (Netherlands). This study was supported by Friedrich Miescher Institute funds; a U.S. Office of Naval Research Naval International Cooperative Opportunities in Science and Technology Program grant; a Marie Curie Excellence grant and a European Union (EU) HEALTH-F2-223156 grant to B.R.; a grant from the EU (RETICIRC) to B.R. and S.P.; grants from the Agence nationale de la recherche (MEDINAS, RETINE) to S.P.; a Center Grant from Foundation Fighting Blindness (U.S.) to S.M.-S. and J.A.S.; grants from the Swiss National Science Foundation and the EU to D.T.; a grant from the EU (TREATRUSH) to J.A.S., S.P., and B.R.; a Marie Curie Postdoctoral Fellowship to D.B.; and a National Centers of Competence in Research Frontiers in Genetics fellowship to V.B. and A.C.G. The Ocular Genetics Unit at Trinity College Dublin is supported by Science Foundation Ireland. The data discussed in this publication have been deposited in NCBI's Gene Expression Omnibus (GEO) and are accessible through GEO Series accession no. GSE22338 (www.ncbi.nlm.nih.gov/geo/query/acc.cgi?acc=GSE22338).

Supporting Online Material

www.sciencemag.org/cgi/content/full/science.1190897/DC1
Materials and Methods
SOM Text
Figs. S1 to S11
Tables S1 to S4
References and Notes

14 April 2010; accepted 11 June 2010
Published online 24 June 2010;
10.1126/science.1190897
Include this information when citing this paper.